Araştırma Makalesi
Adıyaman Üniversitesi
Mühendislik Bilimleri Dergisi
18 (2022) 481-490

NUMERICAL INVESTIGATION OF FLOW CHARACTERISTICS OF A NON-SLENDER LAMBDA WING UNMANNED AERIAL VEHICLE

Haci SOGUKPINAR, Serkan CAG[2*]

[1] Department of Electric and Energy, Vocational School, University of Adiyaman, Adiyaman 02040, Turkey
[2] Department of Machinery and Metal Technology Vocational School, University of Adiyaman, Adiyaman 02040, Türkiye
Geliş Tarihi/Received Date: 09.03.2022 Kabul Tarihi/Accepted Date: 16.09.2022 DOI: 10.54365/adyumbd.1085034

ABSTRACT

In this paper, the low-speed aerodynamic performance of lambda wing with a chord length of c=210 mm and sweep angle of Λ =51°, thickness 3 mm, and beveled leading edges on the windward side with an angle of 58° is investigated numerically. Reynolds Average Navier Stokes (RANS) theorem equations with Spalart-Allmaras turbulence model were solved up to an angle of attack 45° for incompressible flow around the wing surface and, are compared to experiment to corralete simulation precision of computational fluid dynamic approaches. Detail about the aerodynamic performance of lambda wing including development and formation of the leading-edge vortex (LEV), the interaction of flow with the surface, flow separations, and stall are studied, presented, and discussed. LEV was started at 5°, vortex breakdown was observed at halfway along the leading edge at the angle of 20°, finally, by the time angle is 30°, bursting vortex gives a way to stall stage.

Keywords: *LEV, CFD, delta* wing*, lambda* wing*,*

LAMBDA KANATLI BİR İNSANSIZ HAVA ARACININ AKIŞ KARAKTERİSTİKLERİNİN SAYISAL OLARAK İNCELENMESİ

ÖZET

Bu Çalışmada, kiriş uzunluğu c=210 mm, süpürme açısı Λ=51°, kalınlığı 3 mm ve rüzgar yönüne 58° açı ile eğimli hücum kenarına sahip lambda kanadının düşük hızlı aerodinamik performansı nümerik olarak incelenmiştir. Spalart-Allmaras türbülans modeli ile Reynolds Ortalama Navier Stokes (RANS) teorem denklemleri, kanat yüzeyi etrafındaki sıkıştırılamaz akış için 45°'lik bir hücum açısına kadar çözülmüş ve hesaplamalı akışkanlar dinamiği yaklaşımlarının simülasyon etkinliğini doğrulamak için deneysel verilerle karşılaştırılmıştır. Ön uç girdabının (LEV) gelişimi ve oluşumu, akışın yüzey ile etkileşimi, akış ayrımları ve stol dahil olmak üzere lambda kanadının aerodinamik performansı hakkında ayrıntılar incelenmiş ve tartışılmıştır. LEV oluşumu 5°'lik hücum açısında oluşmaya başlamış, 20°'lik eğimde hücum kenarı boyunca yarı yolda girdap kırılması gözlemlenmiş, son olarak hücum açısı 30° olduğunda, stol durumuna geçmiştir.

Anahtar Kelimeler: *LEV, CFD, delta kanadı, lambda kanadı.*

1. Introduction

Lambda wing has aerodynamic superiority compared to another low sweep (Λ<60◦) delta wing, and varied configurations have been preferred for several UCAV projects. Development of new type of unmanned aerial vehicle (UAV) was started in early 2000 which can be used in battle missions while sustaining the low-cost advantage of UAVs [1]. One of the initial research projects was conducted by Boeing for X45-A and later several incremental developments were added and more advanced form like

* e-posta[1] : hsogukpinar@adiyaman.edu.tr ORCID ID: https://orcid.org/0000-0002-9467-2005
e-posta[2] : scag@adiyaman.edu.tr ORCID ID: https://orcid.org/0000-0003-1088-448X

X45-C with lambda wing was created. Shortly after, another Lambda wing version X47-A for the naval mission was developed by US Navy and Northrop Grumman. Conversely, X45-C development continued with NASA for further capabilities and was later named Phantom Ray [2]. Another Lambda wing UCAV project is a French/International program led by Dassault Aviation started in 2003, with the first flight over France in 2012 and lately finished key combat capability and stealth assessments [3]. Taranis is another UCAV project with a modified Lambda wing and projected by BAE Systems in collaboration with many companies. This project was built on experimentation and learning gained from the Taranis and Neuron program [4]. Some other UCAV projects related to lambda wing have been reported in India and China. Aura is an Indian UCAV project and is under development and expected to be operational by 2023 [5]. Lijian (Sharp Sword) is a Chinese UCAV project and is still under development but some of the flight tests were conducted in 2013[6]. Today expectations from UCAV projects are beyond dreams but some of the designs already completed basic combat capability and stealth evaluations. Shortly, UCAV will be replaced by the current warplanes and attract so many g's than manned aircraft with improved combat capability. The Turkish-made UAV TB2 is used actively in Azerbaijan, Karabakh and then in Ukraine, and it is frequently mentioned by changing the war concept of the world. In the last three decades, many theoretical and experimental studies have been conducted to understand the aerodynamic capacity of the delta wing. Vortex development and breakdown is a major steady and unsteady aerodynamic phenomenon for the low sweep delta wings. UCAV aircraft was studied both experimentally and numerically [7]. A wind tunnel observation was managed with the Boeing 1301 UCAV at various angles of attack up to 70 degrees. In the experiment, the stall occurred at the angle of 30° but the stall is not deep, and lift variations continued up to deep stall happened at the angle of 32°. Another Experiment was conducted for the flow field distribution over a lambda wing [8], two types of leading-edge such as sharp and round were implemented to the wing, and pressure and velocity circulation were studied using a Pitot tube and a hot wire anemometer. The sharp edge produced more vortices than the round edge. On the other hand, flow structure on a diamond and lambda wing was investigated by using PIV and dye visualization [9]. In the study, end view streamlines and vorticity pattern were presented and compared for the varying angle of attack. In a similar study [10] end view vorticity pattern was investigated by varying yaw angle from 0° to 20° at the angle of attack up to 35°. As the changing up the yaw angle, flow symmetry distorted continually and in the dispersed windward side, leading-edge vortices covered a majority part of the flow domain. Conversely, on the lee-ward side, leading-edge vortices covered only a small part of the flow domain. Another investigation was performed to investigate the aerodynamic properties of a flying wing configuration [11] as a part of the DLR internal project UCAV-2010. Vortical flow over lambda wing and interactions were investigated for the compressible flow conditions. In another numerical study [12], DLR-F19 lambda model was investigated with two different CFD data and were checked with experimental observation. Lift and drag coefficients and pitching moment coefficient were calculated and checked with numerical methods. The numerical investigation for the flow field over VFE-2 delta wing configuration with rounded leading edges was conducted by using the Cobalt Navier–Stokes solver and dual primary eddy flow topology studied and presented, particularly the sensitivity of the flow concerning the attack angle and Reynolds numbers [13]. In another numerical calculation, Synthetic jet control of the asymmetrical flow field of the flying wing for an UAV was investigated and the study showed that synthetic jet control cannot effectively improve the effect of asymmetrical vortex on the lateral aerodynamic characteristic of the model in zero sideshift [14] on the other hand, in a PIV experiment system, The flow structures and aerodynamic performance of a thin delta wing with a sweep angle of 65 degrees are equipped with needle vortex generators was studied and findings were compared with smooth wing [15] study showed that the acicular wing delays eddy distortion compared to a straight wing. In a wind tunnel experiment, the effect of the thickness-chorus (t/C) ratio on the aerodynamics of a non-thin delta wing with a sweep angle of 45 degrees was characterized and results indicated that the effect of ratio on flow structure was quite substantial [16].

In this study, the flow field pattern of non-slender lambda wing was investigated with numerical methods. For the numerical part, Reynolds Average Navier Stokes (RANS) theorem equations with Spalart-Allmaras turbulence model were solved for incompressible flow around the wing surface and,

are checked with experimental observation [17-21] to validate numerical precision of computational fluid dynamic methods.

2. Numerical approach

Lambda wing UCAV configurations is given in Figure 1. The model has similarity with the X-45C and X-47A UCAV configuration and B-2-type wing platform. The model has a chord length of c=210 mm and sweeps angle of Λ =51°, the thickness of 6 mm and leading edges were beveled as 58°at the windward side and total lower surface area of 251.78 cm^2.

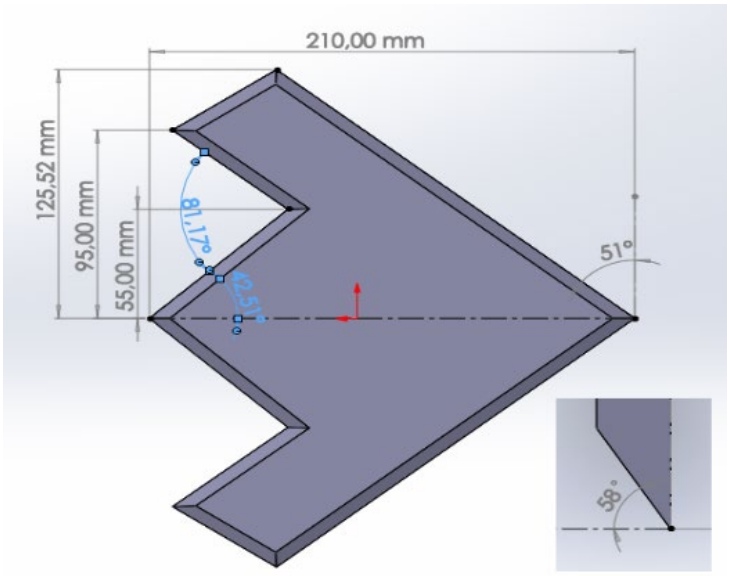

Figure 1. Lambda wing UCAV configurations

The stream solver PARDISO (built into COMSOL) was selected for its performance, robustness, memory efficiency, and easy-to-use software for solving shared memory and distributed-on large systems of sparse symmetric and non-symmetric linear equations. memory multiprocessors. [22]. Spalart-Allmaras turbulence models were used for numerical calculations. This model is also called a low Reynolds number model and does not use wall functions. The model gives satisfying results for many engineering problems, especially airfoil and turbine blade applications where it is calibrated [23]. In this calculation standard version of the Spalart-Allmaras model without the trip term was chosen [23, 24] and the model equation was solved for the undamped turbulent kinematic viscosity-$\tilde{\nu}$ as calculated by Sutherland's (1893) law (1) [25-28].

$$\frac{\partial \tilde{\nu}}{\partial t} = c_{b1}(1-f_{t2})\tilde{S}\tilde{\nu} + \frac{1}{\sigma}\left[\nabla.\left((\nu+\tilde{\nu})\nabla\tilde{\nu}\right) + c_{b2}(\nabla\tilde{\nu})^2\right] - \left(c_{w1}f_w - \frac{c_{b1}}{\kappa^2}f_{t2}\right)\left(\frac{\tilde{\nu}}{d}\right)^2 + f_{t1}.\Delta U^2 \quad (1)$$

The following four terms correspond to production (2), diffusion (3), dissipation (4), and transition (5), respectively.

$$\tilde{S} = S + \frac{\tilde{\nu}}{\kappa^2 d^2}\left[1 - \left(\tilde{\nu}/\nu\right)\left[1 + \frac{\left(\tilde{\nu}/\nu\right)^4}{\left[\left(\tilde{\nu}/\nu\right)^3 + C^3{}_{\nu 1}\right]}\right]^{-1}\right] \quad (2)$$

$$f_w = \frac{\tilde{v}}{\tilde{S}k^2d^2}\left[1 + C_{w2}\left(\left(\frac{\tilde{v}}{\tilde{S}k^2d^2}\right)^5 - 1\right)\right](1 + C_{w3}^6)^{1/6}\left\{\left[1 + C_{w2}\left(\left(\frac{\tilde{v}}{\tilde{S}k^2d^2}\right)^5 - 1\right)\right]^6 + C_{w3}^6\right\}^{-1/6} \quad (3)$$

$$f_{t1} = C_{t1}g_t exp\left[-C_{t2}\frac{w_t^2}{\Delta U^2}(d^2 + g_t^2 d_t^2)\right] \quad (4)$$

$$f_{t2} = C_{t3}exp[-C_{t4}(\tilde{v} / v)^2] \quad (5)$$

The default values for the Spalart-Allmaras modeling parameters are as follows:

$C_{b2} = 0.622,\ \kappa = 0.4187, \sigma = {}^{2}/_{3}, C_{b1} = 0.1355,\ C_{w1} = 3.239,\ C_{w2} = 0.3,\ C_{w3} = 2.0, C_{v1} = 7.1,$ $C_{t1} = 1,\ C_{t2} = 2, C_{t3} = 1{,}2$ and $C_{t4} = 0.5$. For the equations, gravity was included and a no-slip condition was applied on the wing surface. To remove the domain size effect, the simulation area was extended at least 8 times the chord length of the model. The front and backside of the model were extended 12 aerodynamic chord distance, and 8 mean aerodynamic chords up and under the surface of the lambda wing. This configuration is consistent with other numerical studies [7]. The input surface was set to velocity input and the outlet side was set an open surface with zero atmospheric pressure. For the delta wing surface, triangular mesh configuration was selected and minimum mesh size was set to 0.0001 m, and 0.0005 m for maximum. Then for the 3D computational domain, tetrahedral mesh type was preferred with a maximum growth rate of 1.25. The flow field was calculated around 5.9 million cells. Mesh distribution is given in Figure 2. Not half but the full model was simulated under wind speed of 5.2 cm/s at the Reynolds numbers around 10,000. In this study, the mesh distribution was decided by making a comparison in terms of corralation with the experimental and numerical data done before, and compared studies were specified in the references. Since different data were obtained in different mesh applications, this mesh distribution correlates the experimental and numerical image was chosen. In the lower mesh distribution, the results deviate from the experimental comparisons, and in the very high mesh distribution, insolvency occurs.

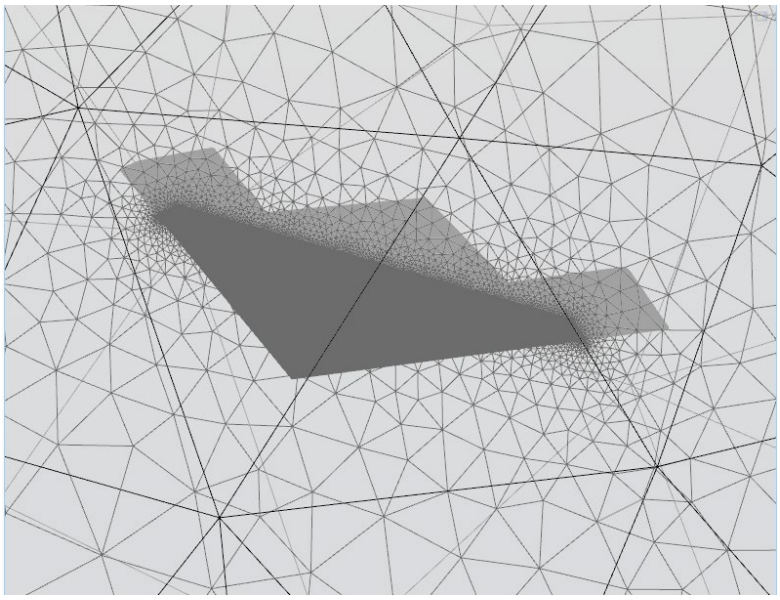

Figure 2. Mesh distribution around the lambda wing

3. Results and Discussion

A series of lower surface flow field patterns and plan view contour vorticity magnitude on the delta wing surface were investigated numerically at varying angles of incidence and are shown in Fig. 3 and Fig.4. At α=5°, the flow is conventional and no turbulence effect is visible in the image. The

vorticity contour image for the same angle confirms that there is no formation of the vortex circulation. This phenomenon is also confirmed with the previously made study [7,29,30]. As the increasing angle of attack to α = 10° (Fig. 3 and Fig.4) most of the flow regimes keep approximately the same pattern with increasing size but a small size LEV is started along the leading edge of the lambda wing. In the streamline velocity image, LEV is developed and circulating along the motion axis. Furthermore, in the vorticity image of the plan view there are two different vortex regions are beginning to appear and the vortices are seen to be rather weak and there are no strong cycles. From these vortex fields, the inner represents primary and the outer vortex represents the minor vortex which is nearer to the leading edge. At α = 15° primary vortex is quite pronounced and circulation is more frequent at the front but less at the back. On the other hand, the secondary vortex is significantly weaker tends to disappear and suggesting breakdown. When α = 20° is reached, the location of the vortex breakdown is approximately halfway along the leading edge and the vortex breakdown location has shifted forward remarkably at the angle of 25°. At α=25°, secondary LEV has already disappeared and as shown in the image of vorticity (Fig. 4 α=25°), there is another vortex region, already formed on the backside of primary vortices. This vortex is called a tertiary vortex and is recorded by Gordnier & Visbal [31] at Re=26 000 at α =15° for a simple delta wing. This type of vortex indicates that the irregularity in the system has increased and the vortex breakdown location is approaching the apex. By the time α=30°, the place of vortex breakdown already reached the apex and bursting vortex slowly changed to a largely stalled lower surface but there is a continuity in the flow indicating that conditions are still creating lift over the lambda wing as given in Fig. 3. Additionally, it is observed that the severity of the tertiary vortex region has increased, and it is completely spread on both sides of the wing in the posterior section as it is shown in the vorticity contour image in Fig.4 (α=30°). At α =35° and above, the symmetrical flow pattern on both sides of the wing is distorted and although the same parameters are defined for both sides, the flow on one side appears to be different on the other side. It is also seen that the LEV axis is curved and divided into two independent vortex regions and a new and powerful new vortex area is formed at the back apex as indicated in Fig.4 (α=35°). At α=35°, LEV axis is completely disappearing and multiple vortex regions appear on the surface this indicates passage of complete stall phase.

Formation and development of a vortex structure in end-view vector and color range velocity field are presented in Fig. 5 where the image was plotted at x/C= 0.2, x/C= 0.4, x/C= 0.8. At the small angles of at α=5°, the color range velocity field indicates there is no significant difference in the velocity distribution of the flow but the vector field shows the rotation of the small-scale flow field at the leading edge. Blue color indicates low speed and higher pressure on the lower surface and reddish color indicates higher speed and creates a lower pressure on the upper surface thus this pressure difference creates a positive lift in the upward direction. As the angle of attack changed to α=10°, small scale LEV development and starts of swirling is evident in every three sections of the image. At the angle of 15°, the size of the vortex and rotation increased compared to the previous image. By the time α=20° is reached, rotation is quite pronounced in the rear section of the image but in the front and middle section size of vortices is low. As it is presented in Fig 3-5 vortex breakdown happened around in the middle part of the lambda wing. Low size vortices in the front and middle section implied vortex breakdown haven't reached these two sections but already passed rear section at the angle of attack 20°. At α=25°, the size of vortices in the middle section increased and almost with the same size as the rear part but in the front, the size of the vortex is weak. As we indicated in the previous Fig. 3-5, location of vortex breakdown has already passed the middle section but the color range difference (velocity difference) on the upper and lower surface indicates lambda wing creating lift near the front of the model. When α=30° is reached, the size of the vortex in the front section catches the size of the other two back section, and the location of the vortex breakdown reached the apex. On the other hand, as is indicated in the previous image in Fig. 3-5, the bursting vortex slowly gives away to the partially stalled phase but the continuity in the flow is partially maintained and this situation creates lift on the UCAV model. Finally, at α=40° and above, rotating vortices on both sides of the surface start to merge and indicate a complete passage of the stall phase.

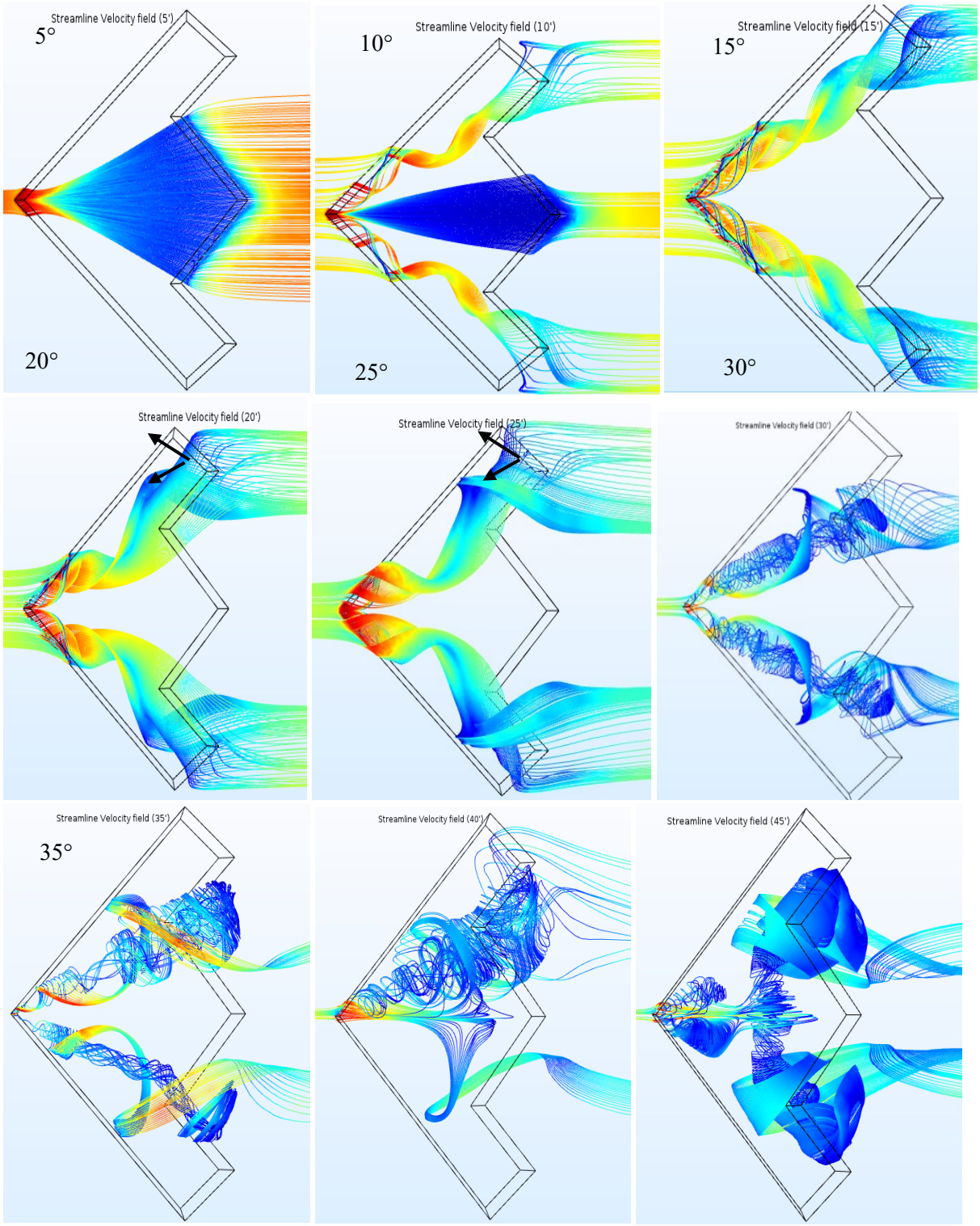

Figure 3. Streamline velocity field on the surface: Formation of the leading-edge vortex, vortex breakdown, and flow separation.

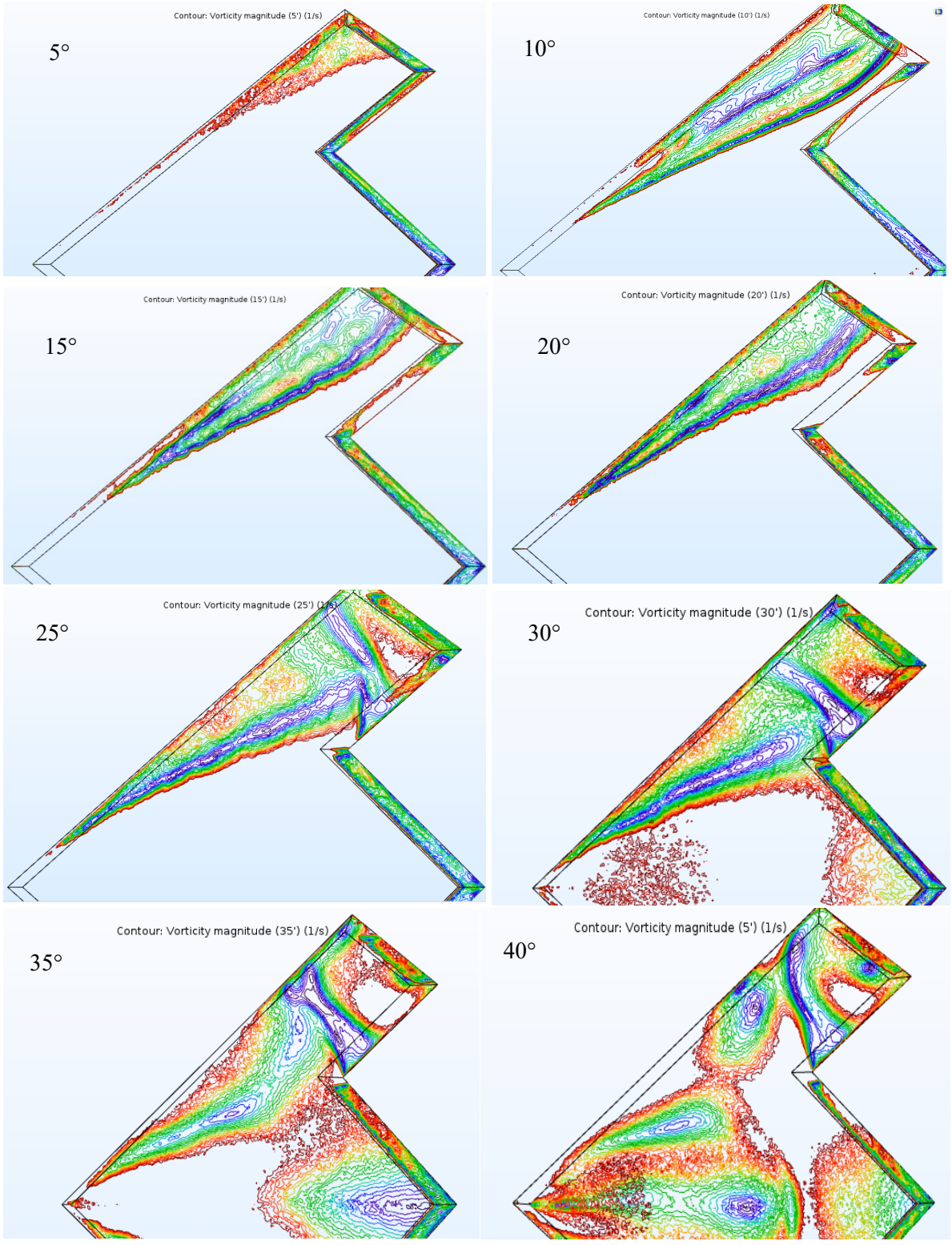

Figure 4. Plain view contour vorticity magnitude on the delta wing surface (1/s)

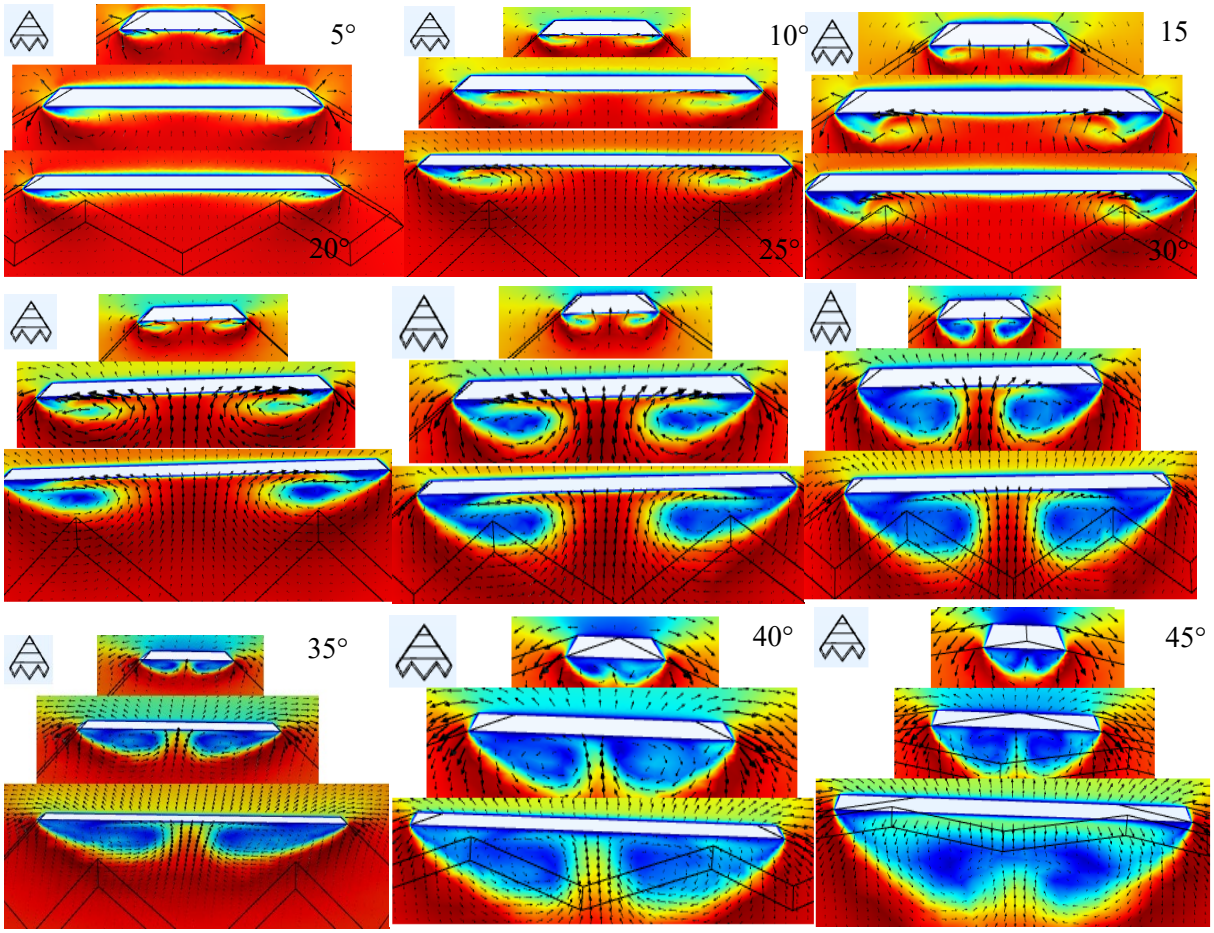

Figure 5. End view vector and velocity field: In the figure upper to lower where x/C= 0.2, x/C= 0.4, x/C= 0.8, when the angle of attack changes from 5° to 45°.

4. Conclusion

A computational study was conducted for unmanned combat aerial vehicles (UCAV) with lambda wing configuration. For the numerical study, Reynolds Average Navier Stokes (RANS) theorem equations with Spalart-Allmaras turbulence model were solved for incompressible flow around the wing surface and, are compared with other study to correlate simulation precision of computational fluid dynamic approaches. The model has a chord length of c=210 mm with a non-slender sweep angle of Λ =51° with a thickness of 6 mm and leading edges were beveled as 58°at the windward side. At the lower angle of attack at α=5°, flow is conventional and no rotation was observed in numerical calculation. As the increasing angle of attack, vortex breakdown happened and the place of vortex breakdown shifted forward up to the apex. By the time α = 30° is reached, vortex breakdown reached the apex and bursting vortices gives a way to stalled phase. This outcome is compatible with a previous study that used a similar lambda configuration [7].

In addition, these results were also compared with the data of another numerical method and although different simulation techniques were used, similar data are obtained. CFD has completed its evolution and has become a valuable tool for design and analysis in an aerodynamic application, and has participated in water channel, wind tunnel and flight testing as a critical tool for initial testing.

Acknowledgment

The authors wish to thank Middle East Technical University for providing technical support

Conflict Of Interest

The authors declare that they have no conflict of interest

References

[1] Sepulveda, E., and H. Smith. "Technology challenges of stealth unmanned combat aerial vehicles." The Aeronautical Journal 121.1243 (2017): 1261-1295.
[2] NASA. Boeing's Phantom Ray Makes First Flight. 2011. Available at: http://www.nasa.gov (Accessed: 11 March 2018)
[3] LARRINAGA N DE., IHS L., WEEKLY D. Neuron completes Italian flight trials. IHS Jane's Defence Weekly. London; August 2015; Available at: http://www.janes.com (Accessed: 11 March 2018).
[4] BEALE J. Top secret UK drone Taranis makes first flight. BBC News. February 2014; Available at: http://www.bbc.co.uk (Accessed: 11 March 2018).
[5] PUBBY M. Government set to clear Rs 3,000 core plan to develop engine for India's first UCAV. The Economic Times. 2015. Available at: http://economictimes.indiatimes.com (Accessed: 11 March 2018).
[6] HSU B. China's 'Sharp Sword' UCAV is Spotted Taxiing. AIN online. May 2013; Available at: http://www.ainonline.com (Accessed: 11 March 2018).
[7] Cummings, Russell M., Scott A. Morton, and Stefan G. Siegel. "Numerical prediction and wind tunnel experiment for a pitching unmanned combat air vehicle." Aerospace Science and Technology 12.5 (2008): 355-364.
[8] Manshadi, M. D., Eilbeigi, M., Sobhani, M. K., Zadeh, M. B., & Vaziry, M. A. (2016). Experimental study of flow field distribution over a generic cranked double delta wing. Chinese Journal of Aeronautics, 29(5), 1196-1204.
[9] Yaniktepe, B., and D. Rockwell. "Flow structure on diamond and lambda planforms: Trailing-edge region." AIAA journal 43.7 (2005): 1490-1500.
[10] Sahin, B., Tasci, M. O., Karasu, I., & Akilli, H. (2017). Flow structures in end-view plane of slender delta wing. In EPJ Web of Conferences (Vol. 143, p. 02099). EDP Sciences.
[11] Huber, K., Schutte, A., & Rein, M. (2012). Numerical investigation of the aerodynamic properties of a flying wing configuration. In 30th AIAA Applied Aerodynamics Conference (p. 3325).
[12] Ghoreyshi, M., Young, M. E., Lofthouse, A. J., Jirásek, A., & Cummings, R. M. (2016). Numerical Simulation and Reduced-Order Aerodynamic Modeling of a Lambda Wing Configuration. Journal of Aircraft, 55(2), 549-570.
[13] Cummings, R. M., & Schütte, A. (2013). Detached-Eddy Simulation of the vortical flow field about the VFE-2 delta wing. Aerospace Science and Technology, 24(1), 66-76.
[14] Xu, X., & Zhou, Z. (2016). Analytical study on the synthetic jet control of asymmetric flow field of flying wing unmanned aerial vehicle. Aerospace Science and Technology, 56, 90-99.
[15] Nematollahi, O., Nili-Ahmadabadi, M., Seo, H., & Kim, K. C. (2019). Effect of acicular vortex generators on the aerodynamic features of a slender delta wing. Aerospace Science and Technology.
[16] Ghazijahani, M. S., & Yavuz, M. M. (2019). Effect of thickness-to-chord ratio on aerodynamics of non-slender delta wing. Aerospace Science and Technology.
[17] Yaniktepe, B., Coşkun Ozalp, and Çetin Canpolat. "Aerodynamics and Flow Characteristics of X-45 Delta Wing Planform." Kahramanmaras Sutcu Imam University Journal of Engineering Sciences 19.1 (2016): 1-10.

[18]Arroyo M.P., Greated C.A. (1991). "Stereoscopic Particle Image Velocimetry "Measurement Science & Technology, Vol.2, No.12, pp.1181-1186.
[19].Westerweel J. (1993). "Digital Particle Image Velocimetry, Theory and Application", Delft University Press,.
[20]. Adrian R. J. (2005). "Twenty Years of Particle Image Velocimetry", Experimental Fluids, Vol.39, pp.159–16.
[21]. Raffel M., Willert, C.E., Wereley, S.T., Kompenhans, J. (2007). "Particle Image Velocimetry: A Practical Guide" 2nd ed., Springer.
[22] Pardiso, "Parallel Sparse Direct And Multi - Recursive Iterative Linear Solvers", User Guide Version 6.0, https://pardiso-project.org [accessed 20 February 2019].
[23] D.C. Wilcox, Turbulence Modeling for CFD, 2nd ed., DCW Industries, 1998.
[24] "The Spalart-Allmaras Turbulence Model," http://turbmodels.larc.nasa.gov/spalart.html. (Accessed: 11 March 2018).
[25] Douvi, C., Eleni T.I., Athanasios, P., Margaris P., "Evaluation of the turbulence models for the simulation of the flow over a National Advisory Committee for Aeronautics (NACA) 0012 airfoil," Journal of Mechanical Engineering Research Vol. 4(3), 2012, pp. 100-111.
[26] COMSOL CFD Module user guide, http://www.comsol.com, 2017
[27] Sogukpinar, H. Low speed Numerical Aerodynamic Analysis of New Designed 3D transport Aircraft. International Journal of Engineering Technologies, 4(4), 153-160.
[28] Sogukpinar, H. (2019). Numerical Investigation of Influence of Diverse Winglet Configuration on Induced Drag. Iranian Journal of Science and Technology, Transactions of Mechanical Engineering, 1-13.
[29] Yayla, S., Canpolat, C., Sahin, B., & Akilli, H. (2013). The effect of angle of attack on the flow structure over the nonslender lambda wing. Aerospace Science and Technology, 28(1), 417-430.
[30] Canpolat, C., Yayla, S., Sahin, B., & Akilli, H. (2009). Dye visualization of the flow structure over a yawed nonslender delta wing. Journal of Aircraft, 46(5), 1818-1822.
[31] Gordnier, R. E., & Visbal, M. R. (2005). Compact Difference Scheme Applied to Simulation of Low-Sweep Delta Wing Flow. AIAA journal, 43(8), 1744-1752.